JOURNAL OF AIRCRAFT
Vol. 41, No. 4, July–August 2004

Aerodynamic Modeling and System Identification from Flight Data—Recent Applications at DLR

Ravindra Jategaonkar,* Dietrich Fischenberg,† and Wolfgang von Gruenhagen‡
DLR, German Aerospace Center, 38108 Braunschweig, Germany

This paper provides an overview of a few selected system-identification activities carried out during the last decade at DLR, the German Aerospace Center. After a brief account of parameter-estimation methods and of consistency checking of recorded flight data, an emphasis is placed on 1) development of global, high-fidelity aerodynamic databases for training simulators; 2) models for in-flight simulator; 3) modeling of stall hysteresis; 4) estimation of aerodynamic flowfield characteristics and validation of aircraft reaction models from wake vortex encounter flights; and 5) a parametric wake distortion model to improve helicopter coupling off-axis response. These examples cover a variety of flight vehicles with widely different characteristics, namely, the military transport aircraft Transall C-160, commuter aircraft Dornier 328, in-flight simulator VFW-614 ATTAS, high-altitude research aircraft G850 Strato 2C, Airbus-type aircraft, fly-by-wire helicopter BO-105, and fly-by-light helicopter EC-135. Besides parameter estimation aspects, those related to model validation are discussed. Through succinct examples it is brought out that system identification has become an indispensable tool to support not only research but also industry activities in various key areas such as model validation, handling qualities evaluation, control law design, and flight-vehicle design and certification. Thus, it contributes significantly to risk and cost reduction.

Introduction

WITH the evolution of modern high-performance aircraft, spiraling developmental and experimental costs, and increasing flight safety issues, the importance of training simulators has steadily increased over the decades.[1] Simulators are increasingly used not only for pilot training, but also for other applications such as flight planning, envelope expansion, design and analysis of control laws, handling qualities investigations, and pilot-in-the-loop studies.[2] Likewise, in-flight simulators provide a reliable, safe, and economical testbed for further investigations, such as flight-control research and system assessment, including means to verify new aircraft design concepts.

The demands of high-performance characteristics have led to aerodynamically unstable aircraft configurations.[3] Accurate models and databases are critical to the design and performance of the mandatory flight-control system over the operational regime.

Wake vortex encounters are critical safety aspects. Optimization of air traffic distribution and volume in the vicinity of airports, particularly under a mix of light, medium, and heavy aircraft, calls for better understanding of the basic physics underlying this phenomenon.[4] For this purpose, validated models for aerodynamic flowfield characteristics and aircraft wake vortex encounter reaction models are indispensable.

Although significant advances have been made to derive high-bandwidth helicopter models by extending the rigid-body model with the rotor dynamics,[5] a long-standing problem in the area of rotorcraft modeling is accurate prediction of off-axis response. The importance of unequal vortex spacing on inflow distribution resulting in a cross-coupling effect as a result of gyroscopic behavior was recognized early this decade.[6] Postulation and validation of such models are imperative.

Received 17 June 2003; revision received 2 September 2003; accepted for publication 2 September 2003.

*Senior Scientist, Institute of Flight Systems, Lilienthalplatz 7. Associate Fellow AIAA.
†Research Scientist, Institute of Flight Systems, Lilienthalplatz 7.
‡Research Scientist, Institute of Flight Systems, Lilienthalplatz 7.

The aforementioned applications demand advanced models and high-fidelity aerodynamic databases of flight vehicles. System identification, which is a scientific approach to modeling from experimental data,[7–9] is extensively and routinely used at DLR to meet these challenging demands by generating validated models and databases from flight data. A listing of the various applications during the last three decades is provided in Table 1 and covers a broad spectrum of more than 40 dynamic systems ranging from simple aircraft to high-performance, highly augmented modern flight vehicles, propulsion, and other aircraft subsystems.[10]

In this paper development of databases for training and in-flight simulators meeting Federal Aviation Administration (FAA) Level-D quality[11] and modeling of complex aerodynamic phenomena such as unsteady flow leading to stall hysteresis, wake vortex encounter, and off-axis response caused by distortion of rotor wake are addressed in some depth. Rigorous treatment of any particular application is sacrificed to cover several examples demonstrating the end use of system-identification results. Through these advanced applications, it is brought out that this methodology, which is an integral part of modeling and simulation (M&S), has become indispensable for flight-vehicle applications because of the complexity of the dynamic system under investigation and also because the benefits derived are substantial.

Parameter-Estimation Methods and Software Tools

Because excellent survey papers and detailed literature on the basic approach to flight-vehicle system identification are already available,[7–9] only a brief account of model formulation and the most commonly used estimation algorithm and its recent extension are presented in this paper. Equations of aircraft motion are formulated in state space as

$$\dot{\boldsymbol{x}}(t) = f[\boldsymbol{x}(t), \boldsymbol{u}(t), \boldsymbol{\Theta}], \qquad \boldsymbol{x}(t_0) = \boldsymbol{x}_0 \tag{1}$$

$$\boldsymbol{y}(t) = g[\boldsymbol{x}(t), \boldsymbol{u}(t), \boldsymbol{\Theta}] \tag{2}$$

$$\boldsymbol{z}(t_k) = \boldsymbol{y}(t_k) + \boldsymbol{v}(t_k), \qquad k = 1, \ldots N \tag{3}$$

where $\boldsymbol{x}$ is the state vector, $\boldsymbol{y}$ the observation vector, and $\boldsymbol{u}$ the control input vector; $\boldsymbol{f}$ and $\boldsymbol{g}$ the nonlinear system functions, and $\boldsymbol{\Theta}$ the q-dimensional vector of unknown parameters. The measurement vector $\boldsymbol{z}$ is sampled at N discrete time points, and the noise vector $\boldsymbol{v}$ is assumed to be a sequence of independent Gaussian random variables with zero mean and covariance matrix R.

Table 1 DLR system-identification experience

Flight vehicle	Period	Type
Civil A/C[a]	1970–1973	Do 27
	1975–1988	HFB 320-S1 FLISI
	1976	CASA C-212
	1978–1983	DHC-2 Beaver
	1981	A300-600
	1982–1985	Do 28 TNT OLGA
	1984	A310
	1986–1996	VFW 614 ATTAS
	1990	DA Falcon E
	1995	Grob G 850 Strato 2C
	1997–1998	Dornier 328-110
	1997	A300-600ST Beluga
	1997–1998	A330-200
	1999–2000	IPTN N250-PA1
	2000	VFW-614 ATD-EFCS
	2001	A340-600
	2002	Dornier-128
	2002	Cessna Citation II
	2002	A318-121
Military A/C and technology demonstrators	1976–1983	MRCA-Tornado
	1977	CCV F 104-G
	1981	Do Alpha-Jet TST
	1984	Do Alpha-Jet-DSFC
	1989–1997	C-160 Transall
	1993–1998	Dasa/Rockwell X-31A
	1997⇒	EF 2000 Eurofighter
	2001 ⇒	X-31A VECTOR
Helicopter and tilt-rotor A/C	1975 ⇒	Bo 105 S123
	1986–1989	Bell XV-15 tilt rotor
	1989–1990	AH 64 Apache
	1989–1990	SA 330 Puma
	1989–1995	Bo 105 S3-ATTHeS
	1998	SA 365 Dauphin
	1999 ⇒	EC 135 HESTOR
A/C models	1978–1980	ATA free-flight model
	1980	Do 28 TNT wind-tunnel model
	1982–1983	Do 28 TNT free-flight model
Reentry models	1989	Falke
	1998	USERS
Parafoil payload	1995	NASA Spacewedge Parafoil
	1997	D 160
	1998 ⇒	ALEX
Rockets and projectiles	1986	EPHAG
	1987–1988	EPHRAM
A/C propulsion systems	1992	Rolls Royce Tyne R.Ty.20 in Transall C-160
	1997	Pratt and Whitney PW 119A in Dornier 328-110
	1997	Rolls Royce M45H MK501 in VFW 614 ATTAS
	1998 ⇒	F404-GE-400 in X-31A
A/C landing gears	1996–1997	C-160 Transall
	1997	Do 328-100
	1997	VFW 614 ATTAS
	1998 ⇒	Dasa/Rockwell X-31A
Miscellaneous	1985	Submarine, Class 206 "U 13"
	1997 ⇒	Aircraft pilot coupling
	1998 ⇒	Combustion plant RWE-VVA

[a] A/C = aircraft.

The maximum likelihood estimates of Θ are obtained by minimizing the cost function[7]

$$J = \frac{1}{2}\sum_{k=1}^{N}[z(t_k) - y(t_k)]^T R^{-1}[z(t_k) - y(t_k)] + \frac{N}{2}\ell_n|R| \qquad (4)$$

The unconstrained Gauss–Newton method yields the iterative parameter update:

$$\Theta_{i+1} = \Theta_i + \Delta\Theta \qquad \text{with} \qquad \Delta\Theta = -F^{-1}G \qquad (5)$$

where the $q \times q$-dimensional information matrix F and the q-dimensional gradient vector G are given by

$$F = \frac{\partial^2 J}{\partial \Theta^2} \approx \sum_{k=1}^{N}\left[\frac{\partial y(t_k)}{\partial \Theta}\right]^T R^{-1}\left[\frac{\partial y(t_k)}{\partial \Theta}\right] \qquad (6)$$

$$G = \frac{\partial J}{\partial \Theta} = \sum_{k=1}^{N}\left[\frac{\partial y(t_k)}{\partial \Theta}\right]^T R^{-1}[z(t_k) - y(t_k)] \qquad (7)$$

The response gradients $\partial y/\partial\Theta$ required to compute F and G using Eqs. (6) and (7) are approximated by using finite differences.[9]

The unconstrained Gauss–Newton method has been recently extended to account for simple lower and upper bounds on the parameters.[12] This leads to linearly constrained optimization problem, formulated as

$$\min J(\Theta) \text{ subject to } \Theta_{\min} \le \Theta \le \Theta_{\max} \qquad (8)$$

An elegant solution to this constrained optimization problem is provided by the active-set strategy. The details of such an algorithm called bounded-variable Gauss–Newton method are elaborated in Ref. 12. It is based on the unconstrained optimization followed by suitably changing the active set as optimization progresses and checking the Kuhn–Tucker optimality conditions whenever the parameter values hit the bounds.

As pointed out in Ref. 12, the computational overhead to implement the active-set strategy in the existing Gauss–Newton method is minor. The advantages of this approach are that the optimization retains the quadratic convergence and the accuracy of the parameter estimates can be readily obtained as in the case of the standard Gauss–Newton method. This algorithm is useful to positively influence the convergence properties as well as to ensure that the parameters are within prespecified bounds, for example, representing certain physical effects.

Besides the two variants of the Gauss–Newton method, the Levenberg–Marquardt algorithm, combining features of the unconstrained Gauss–Newton and the steepest descent methods, is optionally used. It has a wider convergence range and was found useful for starting values far from the optimum. It also overcomes numerical difficulties that might arise as a result of one-sided difference approximation of gradients near the minimum. The direct search algorithms, for example, Simplex or Subplex methods, can sometimes be used to gain some improvement in cases with poor starting values, but are rarely used for large-scale problems because of computational inefficiency.

Measure of Accuracy

Clues into the effectiveness, or lack thereof, of model parameters are necessary to judge the adequacy of identified models and their parameters. The goodness of fit, that is, the cost function value, in this case determinant of the residuals covariance matrix, is a standard criterion.

Yet another form of output statistics for the overall fit is Theil's inequality coefficient (TIC) given by[13]

$$\text{TIC} = \frac{\sqrt{(1/N)\sum_{k=1}^{N}[z(t_k) - y(t_k)]^2}}{\sqrt{(1/N)\sum_{k=1}^{N}[z(t_k)]^2} + \sqrt{(1/N)\sum_{k=1}^{N}[y(t_k)]^2}} \qquad (9)$$

TIC is the ratio of the rms fit error and the rms values of the measured and estimated signals summed together. The main advantage of TIC is that it is a normalized index between 0 and 1; 0 implying perfect fit and close to 1 implying worst case, that is, two time series being significantly different. Acceptable TIC value depends, in general, on the application; however, as a rule of thumb, TIC of 0.25 to 0.3 indicates a good agreement.

The maximum likelihood estimation being asymptotically bias free and efficient, the information matrix F provides a good approximation to the parameter error covariance matrix. The standard deviations of the estimates and the correlation among them are readily obtained from the diagonal and off-diagonal elements of F, respectively. In general, the estimated error bounds are too

optimistic[7]; for realistic, practical conditions they are multiplied by a fudge factor of 5–10.

Software Tools

The standard software tool for system identification at DLR, called ESTIMA, has evolved over the last two decades and is a modular system of high-performance algorithms; optimized and tailored to process large-scale systems and huge amount of measured data.[14] Extensive postprocessing in the time and the frequency domain allow quick evaluation of identified model characteristics. It offers complete flexibility to model arbitrarily complex linear and nonlinear models. The interface is through user subroutines in the Fortran-77 language.

More recently, the basic ESTIMA capabilities have been implemented under MATLAB.® A toolbox, called FITLAB, caters to general nonlinear and linear models written in MATLAB/Simulink.®

Data Consistency Checking

A data compatibility check, sometimes called flight-path reconstruction, ensures that the measurements are consistent and error free. For example, the measured angle of attack must match with that reconstructed from the inertial measurements of accelerations and angular rates. Such a verification is possible in the case of flight data because the well-defined kinematic equations of aircraft motion provide a convenient means to bootstrap the information through a numerical procedure. Because no uncertainties are involved in the kinematic model, a compatibility check provides accurate information about the aircraft states.[15,16] In addition, it provides estimates of scale factors, zero shifts, and time delays in the recorded data. This approach is routinely used to calibrate flow variables from dynamic flight maneuvers.

As an example, calibration of flow angles measured by a five-hole probe mounted on a noseboom on the VFW-614 ATTAS aircraft, (Fig. 1a) is presented.[17] The difference pressures caused by angle of attack and angle of sideslip $p_{d\alpha}$ and $p_{d\beta}$ are modeled as

$$p_{d\alpha} = K_\alpha \bar{q}\alpha_{\mathrm{nb}} + \Delta p_{d\alpha}, \qquad p_{d\beta} = K_\beta \bar{q}\beta_{\mathrm{nb}} + \Delta p_{d\beta} \tag{10}$$

where $\bar{q}$ is the dynamic pressure, K_α and K_β are the unknown sensitivity coefficients per degree, and Δ are the bias corrections in the measurements. The angle of attack and angle of sideslip at the noseboom α_{nb} and β_{nb} are obtained from the local velocity components, computed from the integrated states by accounting for the sensor location away from the center of gravity.

a) Longer noseboom on VFW-614 ATTAS

b) Short noseboom on Transall C-160

Fig. 1 Noseboom-mounted five-hole probe for air data.

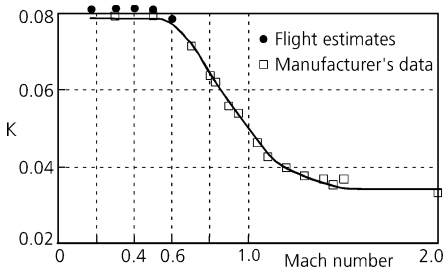

Fig. 2 Comparison of flight-estimated scale factor for VFW-614 with manufacturer's data.

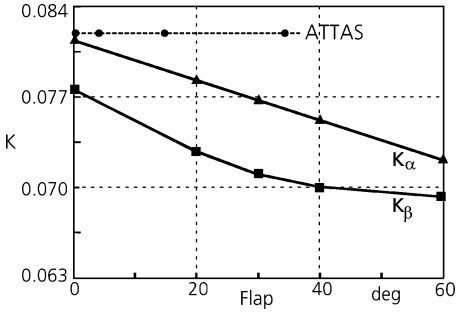

Fig. 3 Flight-estimated calibration factors.

The results of parameter estimation are provided in Fig. 2, which clearly shows that the flight estimates of sensitivity coefficients match reasonably well with the manufacturer's data.[17,18] To summarize, the estimated scale factors for the angle of attack and angle of sideslip are 0.0819 for Mach variation up to 0.55 compared to 0.079 specified by the manufacturer. For Mach 0.6 the scale factor for angle of attack is estimated to be 0.0781, and no Mach dependency could be estimated for angle of sideslip. The minor differences compared to manufacturer's data are attributed to position error, possible errors in measured dynamic pressure, and noseboom length limited to roughly 1.35 times the fuselage diameter, which is probably not sufficient to reach the freestream flow. An empirical rule suggests a boom length of 2.5 to 3 times the fuselage diameter. The sensitivity coefficients were found to be independent of the flap setting and other configuration changes.

The measurement of difference pressure for angle of attack showed a bias of 131 Pa and for the angle of sideslip 200 Pa, resulting mostly from misalignment. As demonstrated in Ref. 17, the time delay in both the measurements was of the order of 130 ms, which was verified in a separate laboratory calibration to result from recording equipment. It is necessary to point out that the scale factors, biases, and time delays are system installation specific. Any generalization to other systems or configurations requires careful consideration.

In yet another case the same five-hole probe was mounted on a shorter noseboom on a Transall C-160 aircraft (Fig. 1b). The estimated parameters are shown in Fig. 3, which clearly shows that the scale factors are configuration dependent. This is attributed to the fact that the noseboom length was just about 0.5 m. It is well known that the flowfield around the aircraft is distorted. A large number of maneuvers were necessary to cover the variations with configuration change.

High-Fidelity Databases for Training Simulators

Although analytical predictions, wind-tunnel measurements on a scaled model, or extrapolation of existing data from similar configurations provide aerodynamic databases valid over the entire flight envelope, they are often associated with certain limitations arising

a) Transall C-160

b) Dornier 328 turboprop commuter aircraft

Fig. 4 High-fidelity databases for training simulators.

from model scaling, Reynolds number, dynamic derivative, and cross-coupling effects. Moreover, in some instances, particularly for the old-generation aircraft, only limited information is available. The importance of flight validation and update of such a database is well recognized. In recent years most aircraft manufacturers consider a simulator data package as an integral part of the aircraft development program.[1] The DLR Institute of Flight Systems is one of the few organizations that supports the aircraft manufacturers in this activity or performs completely on its own the task of generating flight validated fully nonlinear simulation models and databases.

In the recent past, applying system identification methods, aerodynamic databases were generated in several applications,[19–24] specifically at DLR, for the military transport aircraft Transall C-160 (Ref. 22) (Fig. 4a), and the commuter aircraft Dornier 328 (Ref. 24) (Fig. 4b), in both cases meeting the FAA Level D quality criteria.

For Transall C-160, 37 configurations covering five flap settings, three c. g. locations and five different speeds at five altitude levels were tested. Roughly 1000 flight maneuvers were analyzed to derive a rigid-body aerodynamic database valid over the operational flight regime.[22,25] Strong nonlinear effects and dependency of parameters pertaining to the lateral-directional motion on the angle of attack were identified. For example, the yawing moment coefficient is given by

$$C_n = C_{n0} + [C_{n\beta} + C_{n\beta\mathrm{NL}}(\alpha - \alpha_s)]\beta + (C_{\mathrm{np}} + C_{\mathrm{np}\alpha}\alpha)p^* + [C_{\mathrm{nr}} + C_{\mathrm{nrNL}}(\alpha - \alpha_s)]r^* + (C_{n\xi} + C_{n\xi\alpha}\alpha)\xi + (C_{n\varsigma} + C_{n\varsigma\alpha}\alpha)\varsigma \tag{11}$$

where α is the angle of attack, β the angle of sideslip, p^* and r^* the normalized roll and yaw rates, ξ the aileron deflection, ζ the rudder deflection, and C_{ij} the respective unknown aerodynamic derivatives. Nonlinearities in the weathercock stability $C_{n\beta\mathrm{NL}}$ are modeled as

$$C_{n\beta\mathrm{NL}} = \begin{cases} C_{n\beta 1} & \text{for} \quad \alpha > \alpha_s \\ C_{n\beta 2} & \text{for} \quad \alpha \le \alpha_s \end{cases} \tag{12}$$

A similar formulation is also applied to the yaw damping parameter C_{nrNL}. Figure 5 shows a comparison of the analytical/wind-tunnel (WT) predictions with the flight-estimated weathercock stability.

Simulations using the predictions and estimated derivatives are compared in Fig. 6 with the flight-recorded aircraft response for the dutch roll, validation test 2d7 (Ref. 11). The WT predictions yield dutch-roll dynamics having a period of 4.18 s and a damping of 0.207, and the flight-estimated database yields a period of 5.04 s and 0.202 damping factor. A comparison of these values with those approximated from a flight-recorded response (period

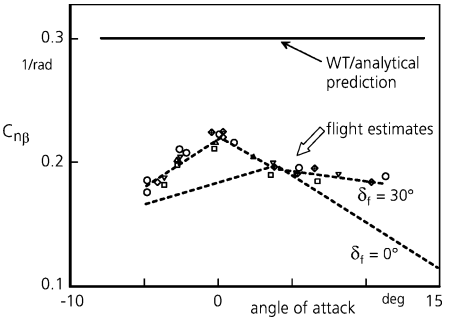

Fig. 5 Transall C-160 Weathercock stability.

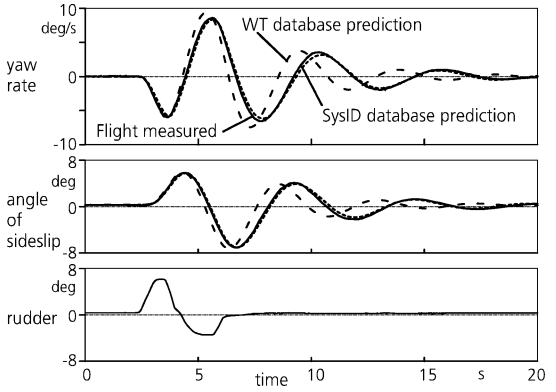

Fig. 6 Validation test for the dutch-roll dynamics of Transall C-160.

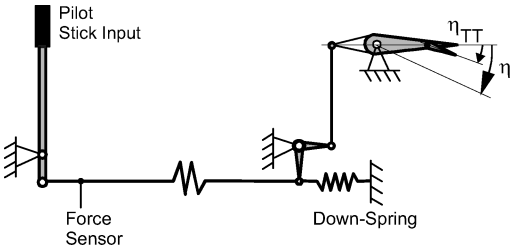

Fig. 7 Schematic of elevator control system.

of 5.12 s and damping of 0.198) clearly demonstrates that only the flight-estimated database meets the FAA tolerances of ±0.5 s or ±10% of period and ±0.02 on damping for this oscillatory mode.

Identification of Hinge Moments

For aircraft with reversible flight controls, in addition to rigid-body aerodynamics it becomes necessary to identify hinge moments for each of the controls. In the case of the high-performance Dornier-328TP, a high-wing, high-tail regional transport turboprop aircraft, roughly 1200 flight maneuvers were analyzed to derive a rigid-body aerodynamic database.[24] It includes the high-angle-of-attack regime with stall hysteresis, large steady sideslip effects, ground effects, and those caused by control-surface malfunctions. The nonlinear influences caused by the propeller slipstream were found to be very predominant. The same set of dynamic maneuvers is analyzed to derive dynamic models including friction and hinge-moment databases for the three primary flight controls.[26] As a typical example, modeling of the elevator flight control is presented in this paper.

In the elevator control system the pilot forces are transmitted from the stick to the elevator by cables and rods (see Fig. 7). The system is preloaded by a downspring. For the dynamic model the mass and moments of inertia of the connecting rods and cables are lumped together with those of the elevator surface (including trim tab) into an equivalent moment of inertia Θ_{elv}. As the pilot force is measured in the first rod, the stick inertia effects are already included in this input signal. This leads to quasi-static transmission of input force to the elevator axis. The elevator dynamics can, therefore, be

formulated as a one-degree-of-freedom system using deflection and deflection rate about the swivel axis as system states[26]:

$$\ddot{\eta} = \tfrac{1}{2}(ME_{\text{elv}} + MF_{\text{elv}})/\Theta_{\text{elv}} \tag{13}$$

where η is the elevator deflection, MF_{elv} the lumped friction moment of the entire elevator control path, and ME_{elv} the sum of all external moments consisting of aerodynamic hinge-moment MH_{elv}, forces transmitted to the aft part, inertia effects caused by dynamic motion, and downspring moment.

The aerodynamic hinge moment MH_{elv} is given by

$$MH_{\text{elv}} = \tfrac{1}{2} C H_{\text{elv}} \bar{q} S_{\text{elv}} \bar{c}_{\text{elv}} \tag{14}$$

where $\bar{q}$ is the dynamic pressure, S_{elv} the elevator surface area, and $\bar{c}_{\text{elv}}$ the elevator reference chord. Without listing all derivatives explicitly, the elevator hinge-moment coefficient was identified as

$$\begin{aligned} C H_{\text{elv}} &= C H_{\text{elv},0}(\alpha_{\text{elv}}, Ma, C_{\text{SP}}, \eta_K) \\ &+ C H_{\text{elv},\eta}(\alpha_{\text{elv}}, Ma, C_{\text{SP}}, \eta, \eta_K) \\ &+ C H_{\text{elv},\eta_{\text{TT}}}(\alpha_{\text{elv}}, Ma, \eta_{\text{TT}}, \eta_K) \\ &+ C H_{\text{elv},\dot{\alpha}}(\eta_K)\dot{\alpha}_{\text{elv}} + C H_{\text{elv},\dot{\eta}}(\eta_K)\dot{\eta}^* \\ &+ C H_{\text{elv},\beta}(\beta_{\text{elv}}, \eta_K) + C H_{\text{elv,GE}}(\eta, \eta_K)\sigma_{\text{elv}} \end{aligned} \tag{15}$$

where the subscript elv denotes variables related to elevator and superscript $*$ the normalized rates.

Without going into any details, it would suffice to say that the elevator hinge-moment coefficient is a function mainly of elevator deflection η, trim-tab deflection η_{TT}, slipstream thrust coefficient C_{SP}, Mach number Ma, flap position η_K, and local flow angles α_{elv} and β_{elv}. The force gradient $C H_{\text{elv},\eta}$ is modeled separately for positive and negative deflections. An angle-of-attack rate influence $C H_{\text{elv}}, \dot{\alpha}$ was found, and aerodynamic damping is provided by an elevator rate term $C H_{\text{elv}}, \dot{\eta}$.

The elevator hinge moment for symmetrical flight was identified by evaluating the dynamic maneuvers (elevator doublets and push-pulls); trims at normal, forward, and aft c.g.-positions; and elevator mistrims. Considering different speed and thrust levels, about 60 maneuvers were analyzed simultaneously for each flap position. The influence of sideslip was identified from steady sideslip maneuvers, and no additional modeling was required for the single-engine cases.

Model Validation

The predictive capability of identified databases is determined by comparing the flight measured aircraft responses with those predicted by the model for the same pilot/control inputs. In this proof of match, the aerodynamic model is kept fixed, and the initial conditions are matched to those in the flight maneuver flown. The subjective evaluation of the quality of match is eliminated through the FAA/JAR (joint aviation requirements) specified guidelines for the tolerances.[11] The flight measurements with these tolerances define a band within which the model response must lie to meet the specified accuracy requirements. For oscillatory modes the tolerances are specified on the frequency and the damping ratio.

For aircraft with reversible flight controls, it is required to demonstrate the adequacy through an end-to-end simulation incorporating both the rigid-body and the hinge-moment databases. In the present case an end-to-end match from force-driven flight controls, providing position-driven rigid-body models, was proved on 170 flight maneuvers specified in the acceptance test schedule and on an additional 1100 maneuvers at other flight conditions, thereby establishing the global validity.[24,26] As a typical example, the case of critical engine failure on takeoff is presented, which pertains to simulation of the response to an engine failure during the high activity task of takeoff, responses to rudder and aileron being of particular interest. Figure 8 shows the results for a few pertinent variables. The complete sequence from stand-still, acceleration, rotation, and climb to 200 ft above ground is simulated as a single maneuver. The results were obtained without any closed-loop control. From the

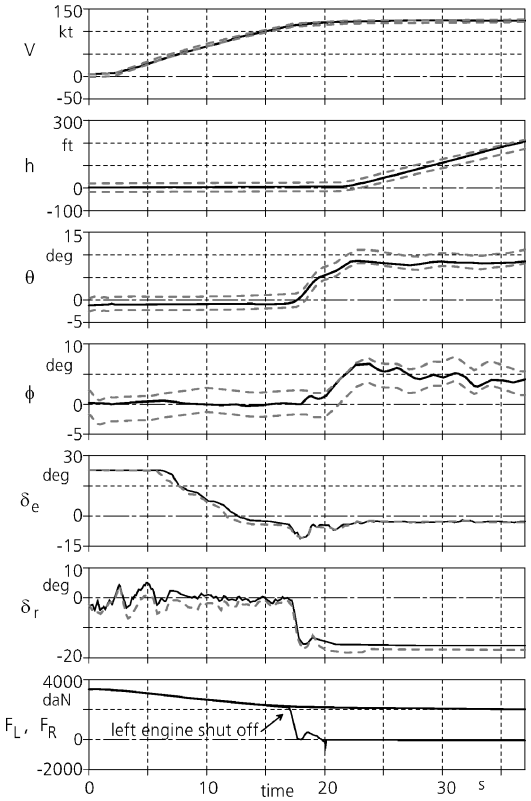

Fig. 8 Proof of match for critical engine failure on takeoff: - - - -, flight measured ± tolerance; and ——, model predicted.

bottom-most plot in Fig. 8 (F_L and F_R, the thrust caused by the left and right engines), it is observed that the critical left engine is shut down immediately after rotation. To maintain the bank and heading, the pilot applies about 15-deg rudder, δ_r in Fig. 8, and about 6-deg ailerons, not shown. Except for a small lead in building up the bank angle, which is still within the tolerance, the match for all of the variables is good. Specifically, the airspeed is within the tolerance of ±3 kn, altitude within ±20 ft, pitch angle within ±1.5 deg and bank angle within ±2 deg. Thus, the database meets the FAA fidelity requirements.

A training simulator for the Transall C-160, incorporating the flight-estimated database, has been operational at the LTG-62 (Air Transport Wing) of the German Air Force at Wunstorf in Germany since 1995. The Dornier 328TP simulators incorporating flight-estimated rigid-body and hinge-moment databases were certified by FAA/JAR-STD and are operational at Dallas, Texas, and Masstricht, The Netherlands, since 1997–1998.

System Identification for Model Following Control

The VFW-614 Advanced Technologies Testing Aircraft System (ATTAS), Fig. 1a, is a fly-by-wire aircraft used for in-flight simulation. In such applications the feed-forward control laws based on the inversion of the mathematical model of the "host" flight vehicle play an extremely important role. This is bacause high-bandwidth control systems need more accurate regulation of initial response than final output error. Accordingly, system identification of ATTAS has been carried out, including the rigid-body model based on wing and tail separately, modeling of direct lift control (DLC), control-surface interference, ground effects, and modeling of actuation systems of primary controls.

The DLC flaps, modified from a part of the landing flaps, are capable of high-frequency direct-lift modulations. They provide an additional independent longitudinal control, which is particularly suitable and necessary for realistic in-flight simulation applications. Rapid and large deflections up to ±35 deg are possible at 75 deg/s under aerodynamic loads. The lift generated by DLC flaps and the

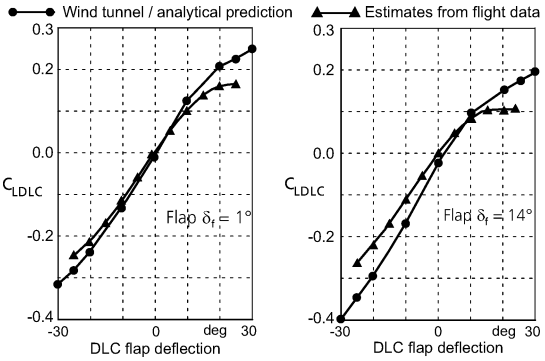

Fig. 9 DLC flaps effectiveness—static characteristics.

resulting pitching moment are modeled as[27]

$$\Delta C_{\mathrm{LDLC}} = A_1\delta_{\mathrm{DLC}} + A_2\delta_{\mathrm{DLC}}^2 + A_3\delta_{\mathrm{DLC}}^3$$

$$\Delta C_{\mathrm{mDLC}} = M_1\delta_{\mathrm{DLC}} + M_2\delta_{\mathrm{DLC}}^2 + M_3\delta_{\mathrm{DLC}}^3 \tag{16}$$

where A_i and M_i are the unknown derivatives that are to be estimated. In addition to the preceding static characteristics, it was found that lag in the downwash generated by DLC flaps affects the pitching motion significantly.[27] This downwash lag effect is modeled as

$$\Delta C_{\mathrm{mDLC}} = C_{L\varepsilon}(r_H/\bar{c})M_\tau\delta_{\mathrm{DLC}}(t-\tau) \tag{17}$$

where $C_{L\varepsilon}$ is the tail lift coefficient, r_H the horizontal distance between the tail and the wing neutral points, and $\bar{c}$ the mean aerodynamic chord. Furthermore, $\delta_{\mathrm{DLC}}(t-\tau)$ is the time-delayed signal, where $\tau = r_H/V$ denotes the transit time required for flow modifications generated at the wing to reach the tail, and M_τ the unknown downwash parameter.

The estimates of DLC flap effectiveness are shown in Fig. 9 (Ref. 27). It is observed that the estimated lift coefficient C_{LDLC} is smaller than the predicted, the difference being pronounced for larger positive deflections. The influence of flow separation for deflections above 10 deg is to be observed. It is clearly evident that the DLC flaps are somewhat less effective in generating direct lift than designed for and predicted from WT tests. The flight-validated static aerodynamic characteristics together with the downwash transient effects provided a high-performance model for the in-flight simulation.

The in-flight simulator VFW-614 ATTAS that incorporates models and database-estimated applying system identification techniques is routinely used for pilot training by the Training School EPNER, Istres, France, and by Empire Test Pilot School (ETPS) Boscombe-Down, United Kingdom. It was recently used for REAL (Robust and Efficient Autopilot Control Law Design) flight testing of advanced autopilot algorithms under the umbrella of a joint project with Airbus France, Airbus Germany, ONERA, and National Aerospace Laboratory, The Netherlands. The most recent application was to support the certification process and the test-pilot first flight training of a new commuter aircraft FD728 JET, a promising project that had to be recently curtailed.

Unsteady Aerodynamic Modeling

Although unsteady aerodynamics has been a subject of extensive investigations using computational-fluid-dynamic methods, wind-tunnel tests, and semi-empirical models, flight validation of the postulated models had been difficult in the past. The recent advances in aerodynamic modeling have led to analytical models for complex processes such as ground effects and separated flow including stall hysteresis, making amenable identification and validation from flight data.

Based on the Kirchhoff's theory of flow separation, the wing lift can be modeled as a function of angle of attack α and flow separation point X (Refs. 28 and 29):

$$C_L(\alpha, X) = C_{L\alpha}\left\{(1+\sqrt{X})/2\right\}^2\alpha \tag{18}$$

where $C_{L\alpha}$ is the lift-curve slope and $X(0 \le X \le 1)$ is a dynamic variable describing the instantaneous location of the flow separation point along the chord on the upper surface of the wing, and $X = 1$ and 0 correspond to attached and fully separated flow, respectively. Considering simplified expressions, the total drag and pitching-moment coefficients are modeled as

$$C_D = C_{D0} + \frac{1}{e\pi\Lambda}C_L^2(\alpha, X) + \frac{\partial C_D}{\partial X}(1-X) \tag{19}$$

$$C_m = C_{m0} + C_m\alpha + C_{m\delta e}\delta_e + \frac{\partial C_m}{\partial X}(1-X) \tag{20}$$

where Λ is the wing aspect ratio, e the Oswald factor, and δ_e the elevator deflection. The major contribution to the unsteady drag comes from the drag polar using $C_L(\alpha, X)$, the lift modified as a result of flow separation. Any additional effects are accounted for through an empirical correction term $\partial C_D/\partial X$. The parameter $\partial C_m/\partial X$ models the hysteresis effect in the pitching moment.

The flow separation point X can be determined from wind-tunnel tests or can also be identified from flight-test data using the approximation

$$X = \tfrac{1}{2}\left\{1 - \tanh[a_1(\alpha - \tau_2\dot{\alpha} - \alpha^*)]\right\} \tag{21}$$

where $\dot{\alpha}$ is the rate of change of angle of attack, τ_2 the time constant accounting for the unsteady aerodynamic effects, α^* the breakpoint for $X = 0.5$, and a_1 the airfoil static-stall characteristics. The time constant τ_2 depends on airfoil section and wing configuration. The three parameters a_1, τ_2, and α^* are completely adequate to model the stall hysteresis. Further extensions to model time-dependent flow separation are possible based on an approximation of the Wagner or Theodorsen function.[30]

The parameters of the unsteady aerodynamic model for flow separation and stall were identified from flight data for several aircraft. As a typical example, Fig. 10 shows a comparison of the total lift and pitching-moment coefficients derived from flight-measured data (shown by solid lines) with those estimated using system identification (shown by dashed lines) for the Dornier 328 aircraft flying a stall maneuver with quasi-steady approach.[24] The increment in pitching moment caused by unsteady aerodynamics, leading to hysteresis, is plotted separately in Fig. 10 (shaded area). The efficacy of the analytical model postulate is evident from the hysteresis in the lift and pitching-moment coefficients.

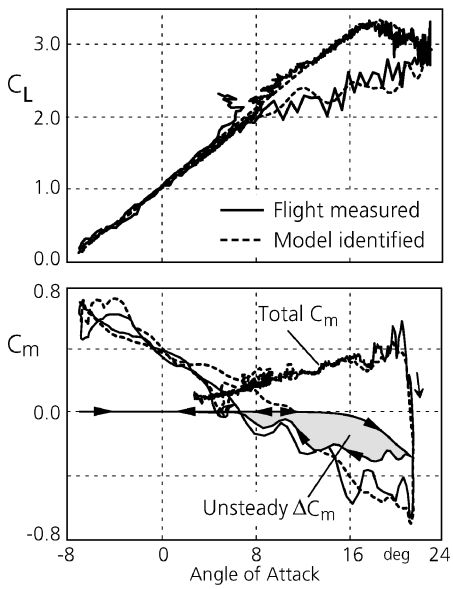

Fig. 10 Modeling of Dornier 328 stall hysteresis.

Such flight-validated stall models are incorporated in the aerodynamic databases for the aforementioned Level D training simulators Transall C-160 and Dornier 328 and the in-flight simulator ATTAS. The same approach was also applied to the X-31A poststall maneuvering program covering up to 70-deg angle of attack. Accurate stall modeling leads to an effective flight crew training on a simulator under extreme flight conditions with flow separation, and meets the recent recommendations made by the National Transportation Safety Board after a Jetstream 4101 aircraft crash following a stall caused by improper pilot reaction to stall warning.[31]

X-31A Unstable Aircraft System Identification

The U.S./German technology demonstrator X-31A successfully established the poststall maneuvering using thrust vectoring.[3,32] Analysis of X-31A flight data enabled unique experimental and estimation techniques for unstable systems.[32] Reference 9 provides a brief account of intricacies and subtleties involved and problems encountered in the parameter estimation of an unstable aircraft that can be flown only in closed loop with the aid of highly complex flight-control laws. A variety of algorithms in the time domain (artificially stabilized output-error method, filter-error method, equation decoupling, regression analysis, and extended-Kalman-filter technique) were applied in this case.[9,33]

System-identification techniques provided improved results for flight-test planning, flight envelope expansion, and a database for simulation and control law modification and validation.[9,32] These techniques continue to be applied to the successor project X-31 VECTOR now under progress, details of which are left to another dedicated paper in this issue.

High-Altitude Research Aircraft Strato 2C

The largest all-composite aircraft ever built, Strato 2C, was designed for high-altitude research, enabling study of ozone depletion and other atmospheric conditions. Designed to cruise at high altitudes for 48 hours,[34] the two-propeller test aircraft (Fig. 11), reached 60,867 ft during the testing phase. Special dynamic maneuvers for parameter estimation (PID) were performed during the flight tests, covering a speed range of 55–90 knots indicated airspeed (KIAS) and altitudes up to 30,000 ft. These maneuvers consisted of multistep 3211 elevator inputs exciting the short period motion, step inputs exciting the phugoid mode, aileron inputs exciting the rolling motion, and rudder doublets exciting the dutch roll.

Through flight-path reconstruction the flow sensor signals (dynamic pressure, angle of attack, and angle of sideslip) were calibrated prior to aerodynamic model identification. Trailing cone measurements were used to calibrate the dynamic pressure.

During the parameter estimation, it was found necessary to properly account for the reaction moments and also the gyroscopic moments caused by two rotating propellers. A database valid for a flight envelope up to 30,000 ft, low-speed aerodynamics and incompressible flow without aeroelastic and Reynolds-number effects was determined from flight data applying the maximum likelihood parameter estimation method.[35] For the investigated flight regime the lateral aerodynamic model showed a strong dependency on the angle of attack. The rolling moment coefficient was modeled as

$$C_l = C_{l0} + C_{l\beta}\beta + (C_{l_p} + C_{l_{p\alpha}}\alpha)p^* + C_{lr}r^* + (C_{l\xi} + C_{l\xi\alpha}\alpha)\xi + C_{l\zeta}\zeta \tag{22}$$

Fig. 11 High-altitude research aircraft Strato 2C.

With increasing angle of attack, Strato 2C has a considerable decrease in aileron effectiveness as well as decrease in roll and yaw damping. The flight-estimated aerodynamic derivatives were used to verify and update the predictions for handling qualities evaluation and for improved simulation purposes.

Wake Vortex Aircraft Encounter Model

Aerodynamic interaction models (AIM) are an indispensable part of flight mechanic simulation models concerned with wake vortex encounter investigations, for example, simulator studies or encounter risk assessment. Two typical AIMs are the strip method and the lifting surface method.[36,37] Both can be adapted to various aircraft configurations and compute the wake vortex flowfield induced additional forces and moments that are added to the forces and moments computed by the basic aircraft aeromodel. For reliable simulation results the quality of the AIM model is of prime importance. Up to now, quality has often been proven by comparing model forces and moments to static wind-tunnel measurements, in which the follower aircraft is set to distinct positions behind a wake-generating configuration.

Within the fifth European framework technology project S-WAKE,[37] one objective is to validate the AIMs using data of full-scale flight tests, which were carried out with three aircraft: ATTAS, a Do-128, and a Cessna Citation. A task of the leading aircraft ATTAS (ICAO separation class: medium) was to visualize the wake with a wing-mounted smoke generator. The follower aircraft (separation class: light) encountered the ATTAS wake at different, distinct horizontal distances (Fig. 12). Both follower aircraft were fully instrumented with inertial sensors and several flow probes (Do-128) in order to measure the flowfield characteristics of the wake vortex as well as the aircraft response during each encounter. About 100 encounters were flown under steady atmospheric conditions, and bank angles up to 80 deg could be observed, with typical bank angles of 30–40 deg during a lateral encounter.

Determination of Flowfield Characteristics

Precise determination of the flowfield characteristics to which the follower aircraft is subjected to during each of its individual encounters is a prerequisite and critical to aerodynamic encounter model validation. Two different analytical velocity distributions (Burnham–Hallock and Lamb–Oseen) were investigated to match the measured flowfield characteristics.[38,39] First, the flight path was reconstructed precisely using system-identification techniques. Then, the parameters of the analytical wake vortex model were identified.[40] The model consists of two idealized, superimposed counter-rotating single vortices (Fig. 13), characterizing the aircraft wake vortex system after wake roll up. The model parameters are vortex circulation Γ, core radius r_C, lateral vortex separation b_V, and vortex location in space. The tangential velocity of one vortex as a function of the distance from the core $V_t(r)$ is described in terms of the circulation Γ and the core radius r_C:

Lamb–Oseen:

$$V_t(r) = \Gamma/2\pi r\left(1 - e^{-1.2544\,r^2/r_c^2}\right) \tag{23}$$

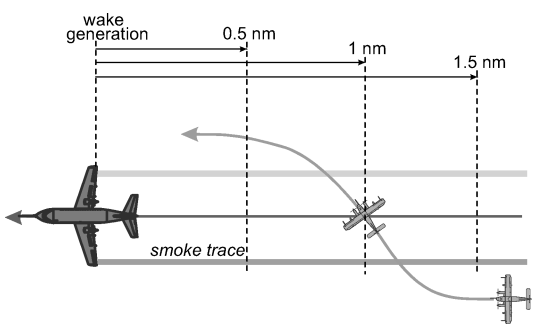

Fig. 12 Schematic of encounters flown.

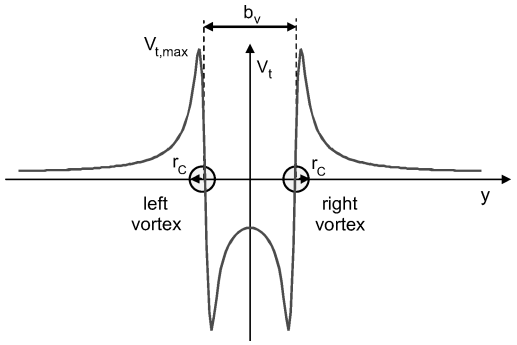

Fig. 13 Analytical wake vortex model.

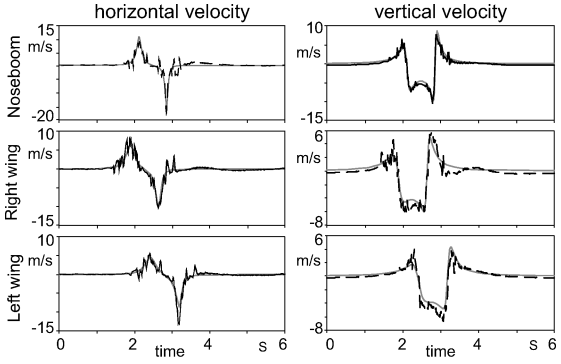

Fig. 14 Wake velocity components during lateral encounter: ----, measured; and ——, Burnham–Hallock model.

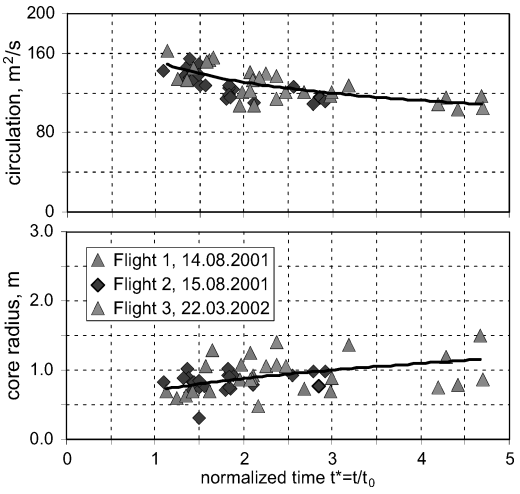

Fig. 15 Flight-estimated vortex model parameters for Burnham–Hallock velocity distribution.

Burnham–Hallock:

$$V_t(r) = \Gamma/2\pi\left[r\Big/\left(r_c^2 + r^2\right)\right] \tag{24}$$

Both vortex models allow computation of flow measurements for most wake vortex ages. As an example, Fig. 14 shows the match of the measured velocity components from three flow probes during a Do-128 lateral wake encounter, 0.53 n miles behind ATTAS.[40] In this plot it can be seen that the encounter is flown from the left to the right, as the right-wing sensor enters the flowfield first, followed by the center-mounted noseboom sensor and then the left-wing sensor. In general, compared to the Lamb–Oseen, the Burnham–Hallock model is slightly better suited to characterize the wake-induced velocities, especially close to the vortex core with high gradients.

Figure 15 summarizes the identified core radius and circulation of the Burnham–Hallock model for Do-128 encounters from three

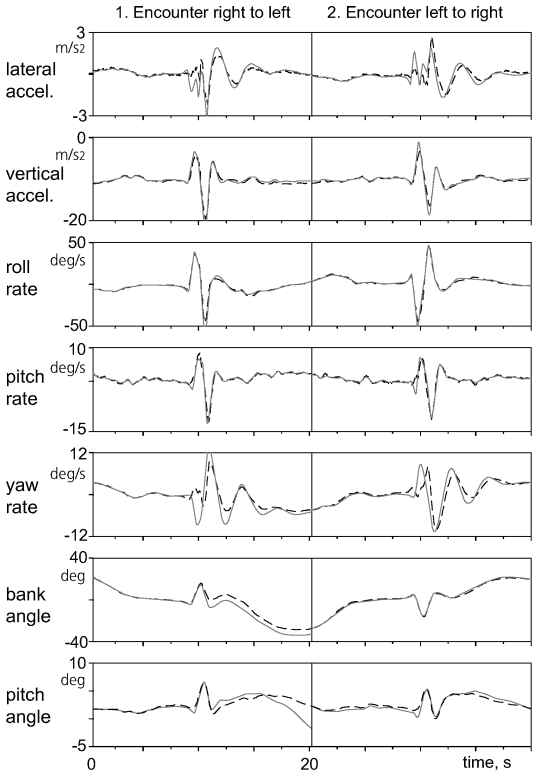

Fig. 16 Strip method validation of two typical lateral Do-128 encounters: ——, flight measured; and ----, simulation model.

flights. The estimates are plotted as a function of normalized time $t^* = t/t_0$, which indicates the vortex age ($t_{0,\mathrm{ATTAS}} = 11$ s). In conformance with the theory, Fig. 15 shows the expected decay of circulation, as well as the increase of the core radius. The initial core radius is about 0.75 m, which is 3.5% of the wake-generating wing span; it is somewhat smaller than the commonly stated value of 5%.

Validation of Aerodynamic Interaction Model

Validation of the strip method is presented in this context. It accounts for incremental aerodynamic forces and moments induced by the wake vortex flowfield.[36] These are added to the basic aircraft forces and moments. For validation, the just determined vortex characteristics and the measured control-surface deflections were used as inputs.[37] For the Do-128 aircraft the wing and the horizontal and vertical tail are divided in total 28 strips: wing, 16 and tail, 12. Flowfield-induced incremental angles of attack and therefrom resulting incremental lift are computed for each strip. Integrating all the single strip forces, the total forces and the moments are obtained.

In Fig. 16 typical model outputs are compared to the corresponding measured values. The most important model outputs for risk assessment (vertical acceleration, roll rate, and bank angle) are computed with very good accuracy. The pitching motion is represented in good quality too. Some systematic deficiencies are observed in the side force (lateral acceleration) and yawing motion, probably because of missing fuselage effects in the strip model. The simple strip method seems to be fairly adequate for flight mechanic encounter modeling. It should be noted that these results were obtained with a relatively simple aircraft configuration (rectangular wing planform). Aircraft with, for example, wing sweep, can be simulated with lesser quality using this method.

Identification of Flexible Aircraft

As a part of overall verification of flight mechanical parameters, system-identification techniques are applied to determine the aerodynamic derivatives of Airbus aircraft, A330-200, A340-600, and A318-121. These estimates obtained by independent groups applying different analysis techniques are compared against each other and used in the certification procedure.

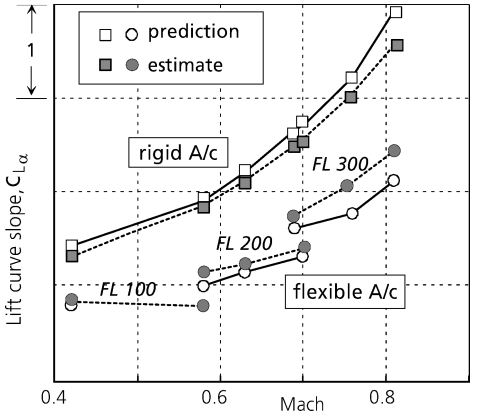

Fig. 17 Flight-estimated and predicted lift-curve slopes of a typical large transport aircraft.

The flight tests were carried out by Airbus, exciting the short period motion, rapid roll, and dutch roll as well as steady sideslip maneuvers. The multistep control inputs suitable for system identification were applied through an onboard computer. Having verified the consistency of recorded flight data, the standard output-error parameter-estimation method is applied to estimate the aerodynamic derivatives pertaining to the longitudinal and lateral-directional motions.

Classical pointwise identification yields stability and control derivatives related to a specific trim condition. The estimated parameters are the sum of all influences, for example, Mach effects or structural deformation. The influence of the latter one is often predicted as a function of dynamic pressure. In flight mechanic simulations, even for large transport aircraft, the influence of structural deformation can be described in a quasi-steady manner, provided the rigid-body and structural frequencies are sufficiently separated. Thereby the complex generalized equations of motion are avoided. Each derivative C_i is formulated as the sum of the rigid-body derivative (for dynamic pressure $\bar{q} = 0$) and a dynamic pressure dependent part, which is mostly described in a linear form through a flex factor k.

$$C_i(\bar{q}) = C_i(1 + \bar{q}k_i) \tag{25}$$

Concatenating flight maneuvers at several selected flight conditions, the dynamic pressure-dependent quasi-steady effects caused by structural deformation and rigid-body aerodynamic derivatives can be separated and determined using system-identification methods. For this, Mach-number dependency must be known or is identified with a Prandtl–Glauert formulation.[41,42] Figure 17 shows the lift-curve slope for a large transport aircraft, showing the Mach-dependent, rigid-body part ($\bar{q} = 0$), as well as the derivative with dynamic pressure influence. Prediction and flight estimates show a reasonable fit. Other parameters, for example, damping and control derivatives, often show somewhat larger discrepancies between predictions and flight estimates, as structural influences for these derivatives are much more complex to predict and might be nonlinear.

Rotor Wake Modeling

During roll and pitch maneuvers in hover and at low speeds, unsymmetrical vortex compression and dilatation act on the induced velocity field in the proximity of the main rotor. These act on the effective angle of attack at the blade sections, which directly affect the aerodynamic rotor loads. The gyroscopic behavior of the rotor caused by the blade flapping dynamics forced by these loads leads to strong cross-coupling effects of the helicopter as a result of the wake distortion. Development of suitable flight dynamic models describing this phenomenon is a current research topic in rotorcraft modeling to obtain improved simulation fidelity in off-axis response.

The helical vortex sheet and blade tip vortex propagation can be either described by geometrically prescribed or free wake formulation with discrete vortices or with an equivalent vortex ring/sheet formulation. Figure 18 shows the principle of a pitching helicopter in hover.

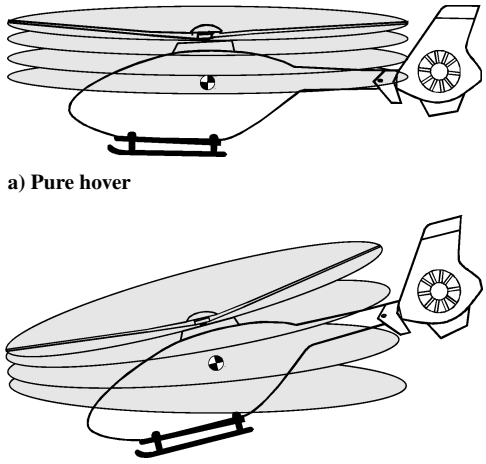

a) Pure hover

b) Pitching motion in hover

Fig. 18 Schematic of wake propagation.

The just-mentioned models require an extensive and complex formulation for the aerodynamics within the flight dynamics model. For various applications a less complex model is more appropriate. By analysis of the local phenomena with respect to their global effect on the helicopter dynamic response, it is possible to parameterize them and formulate a global model associated with the dynamics of the inflow. One possible approach is a parametric extension of the Pitt and Peters dynamic wake model, which can be represented as[43–45]

$$\underline{M}\dot{\underline{\lambda}} + \hat{\underline{L}}^{-1}\underline{\lambda} = \underline{c} + \frac{1}{\Omega}\hat{\underline{L}}^{-1}\begin{bmatrix} 0 \\ K_p(p - \dot{\beta}_s) \\ K_q(q - \dot{\beta}_c) \end{bmatrix} \tag{26}$$

where $\underline{M}$ is the apparent mass matrix associated with the acceleration term from momentum theory, $\hat{\underline{L}}$ the gain matrix, $\lambda(=[\lambda_0, \lambda_s, \lambda_c]^T)$ the inflow ratio describing the first harmonic terms, $c(=[c_T, c_l, c_m]^T)$ the rotor load coefficients with respect to rotor thrust and aerodynamic pitch and roll moment, Ω the main rotor rotation speed, K_p and K_q the wake distortion parameters for lateral and longitudinal distribution of the induced velocity, and $\dot{\beta}_s$ and $\dot{\beta}_c$ the lateral and longitudinal flapping rates. The last term on the right-hand side of Eq. (26) is the parametric term that feeds back the total roll and pitch rates of the rotor tip-path plane with respect to the surrounding air to the induced velocity distribution over the rotor disk. The wake distortion parameters can either be estimated by linearization of the nonlinear formulation or determined by system-identification techniques.

Investigations were carried out for hover and forward flight using BO-105-S123 helicopter flight data. As a typical example, Fig. 19 shows two maneuvers, the first with a longitudinal and the second with a lateral pilot input, here the corresponding blade root measurements are depicted. The model response without wake distortion shows considerable discrepancies compared to the measured data, particularly in the off-axis response of pitch rate resulting from lateral input. Substantial improvements in the axis coupling predictions are obtained by estimating optimal values for the wake distortion parameters K_p and K_q.

The results shown in Fig. 19 are derived based on a rotor model with a single flapping mode and shows the optimum achievable with the model complexity used. Although the basic response characteristics are fairly well captured by the preceding model extension, some deviations in the amplitude resulting from dynamic input are observed. Recent investigations have demonstrated that higher-order free wake models and more blade deflection modes lead to further improvements in the on- as well as off-axis response predictions.[46] Although the preceding investigations have been carried out with a

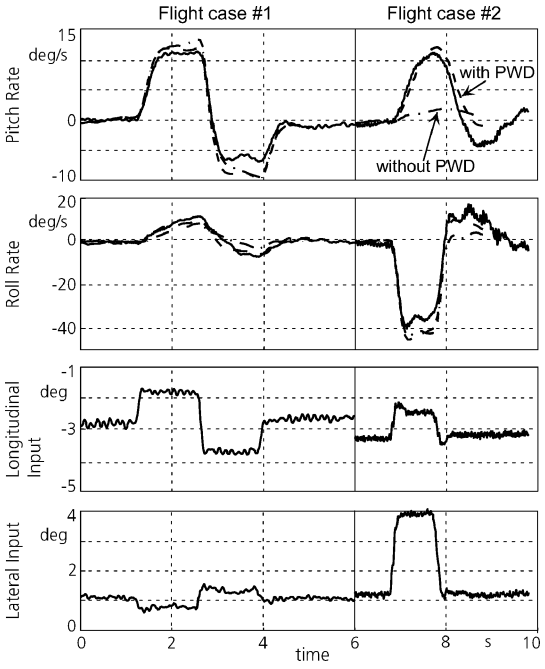

Fig. 19 Improvement of simulation fidelity by parametric wake distortion (PWD) model: ——, flight data; and - - - -, model.

Fig. 20 EC-135 FHS—Flying Helicopter Simulator.

BO-105 helicopter, the modeling aspects are general enough to be valid for other rotorcraft as well.

Just recently, applying system-identification methodology, flight-validated models of an EC-135 helicopter, (Fig. 20), have been derived both for rigid-body aerodynamics and for high-bandwidth control applications. For this purpose a comprehensive flight-test program was carried out, with multistep and sweep control inputs. As a typical example, the predictive capability of rigid-body model identified at 60 kn forward speed is demonstrated in Fig. 21 for two flight maneuvers, namely, lateral and pedal input, respectively. As already pointed in one of the foregoing sections, for such validations only the trim conditions are matched, keeping the aerodynamic model fixed. Identification of aerodynamic database at this flight condition was based on a multiple run analysis in the time domain concatenating several dynamic maneuvers as well as frequency sweeps with longitudinal, lateral, collective, and pedal inputs. Moreover, the aerodynamic model incorporated angle-of-attack dependent derivatives pertaining to the lateral directional motion and also nonlinear effects, for example, the weathercock stability $C_{n\beta}$ being different for positive or negative angles of sideslip. As seen from Fig. 21, the prediction for supplementary data, that is, flight maneuvers not used in aerodynamic identification, is fairly good. The current effort is concentrated on identifying the model at hover. The EC-135 is the basis of DLR's new Flying Helicopter Simulator, which is used for evaluating advanced helicopter control concepts and demonstration of new technologies for future rotorcraft. High-fidelity models are a prerequisite for these applications and for ground-based simulator.

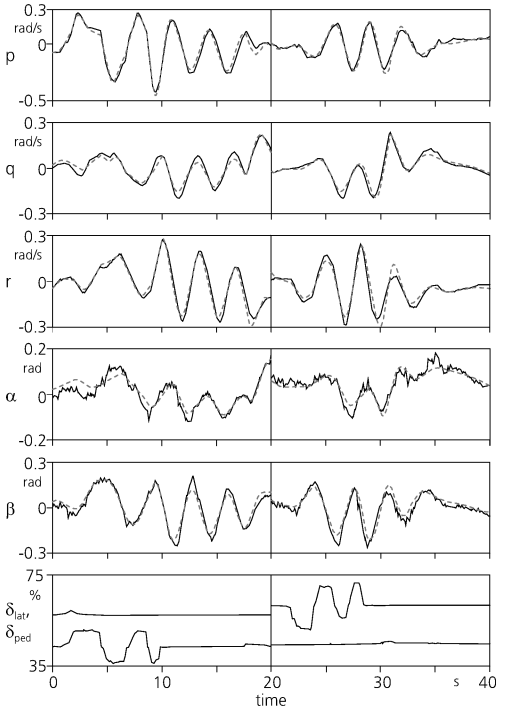

Fig. 21 EC-135 model predictive capability: ——, flight data; and - - - -, model.

Conclusions

To start, a brief account is provided of 1) recent additions to the aircraft parameter-estimation methods and criteria to judge model adequacy in terms of residuals and 2) an example of flight-path reconstruction bringing out the need for careful calibration of flow angles that can be configuration dependent for sensors mounted on a short boom. This is followed by three examples of aerodynamic database development for high-fidelity requirements of training simulators and model following control. A brief description is provided of 1) unstable aircraft identification, 2) high-altitude research aircraft, 3) validation of flight mechanical parameters for certification purposes, and 4) parametric extension of a dynamic wake distortion model, yielding improved off-axis helicopter response. In some depth modeling of unsteady aerodynamics and stall hysteresis from flight data is dealt with. Likewise, estimation of flowfield characteristics and validation of an aircraft reaction model for wake vortex encounters are elucidated. In each reported example the need for flight-estimated models and the end use of such models derived by applying system-identification techniques have been clearly brought out. Through a wide variety of advanced applications, it is unambiguously shown that flight-vehicle system identification is a highly powerful, useful, and indispensable tool.

References

[1]Allen, L. D., "Evolution of Flight Simulation," AIAA Paper 93-3545, Aug. 1993.

[2]Norton, W. J., "Balancing Modeling and Simulation with Flight Test in Military Aircraft Development," AGARD CP-593, Dec. 1997, pp. 13.1–13.25.

[3]Ross, H., "X-31 Enhancement of Aerodynamics for Maneuvering Beyond Stall," AGARD CP-497, Nov. 1991, pp. 2.1–2.12.

[4]Vicroy, D., Brandon, J., Greene, G., Rivers, R., and Stewart, E., "Characterizing the Hazard of a Wake Vortex Encounter," AIAA Paper 97-0055, Jan. 1997.

[5]Hamel, P., and Kaletka, J., "Advances in Rotorcraft System Identification," *Progress in Aerospace Sciences*, Vol. 33, Nos. 3–4, March–April 1997, pp. 259–284.

[6]Rosen, A., and Isser, A., "A Model of the Unsteady Aerodynamics of a Hovering Rotor that Includes Variations of the Wake Geometry," *Journal of the American Helicopter Society*, Vol. 40, No. 3, 1995, pp. 6–16.

[7]Maine, R. E., and Iliff, K. W., "Identification of Dynamic Systems—Applications to Aircraft. Part 1: The Output Error Approach," AGARD, AG-300, Vol. 3, Pt. 1, Dec. 1986.

[8]Klein, V., "Estimation of Aircraft Aerodynamic Parameters from Flight Data," *Progress in Aerospace Sciences*, Vol. 26, No. 1, 1989, pp. 1–77.

[9]Hamel, P. G., and Jategaonkar, R. V., "Evolution of Flight Vehicle System Identification," *Journal of Aircraft*, Vol. 33, No. 1, 1996, pp. 9–28.

[10]Hamel, P. (ed.), "Art and Science of System Identification," *The Challenge of Flight Research—A Historical Account and Technical Guide*, DLR IB-111-99/02, Braunschweig, Germany, 1999, pp. 69–78.

[11]"Airplane Simulator Qualification," Federal Aviation Administration, Advisory Circular, AC 120-40C, Washington, DC, Jan. 1995.

[12]Jategaonkar, R. V., "Bounded Variable Gauss-Newton Algorithm for Aircraft Parameter Estimation," *Journal of Aircraft*, Vol. 37, No. 4, 2002, pp. 742–744.

[13]Murray-Smith, D. J., "Methods for the External Validation of Continuous System Simulation Models: A Review," *Journal of Mathematical Modelling of Systems*, Vol. 4, No. 1, 1998, pp. 5–31.

[14]Jategaonkar, R. V., and Thielecke, F., "ESTIMA—an Integrated Software Tool for Nonlinear Parameter Estimation," *Journal of Aerospace Science and Technology*, Vol. 6, No. 8, 2002, pp. 565–578.

[15]Klein, V., and Schiess, J. R., "Compatibility Check of Measured Aircraft Responses Using Kinematic Equations and Extended Kalman Filter," NASA TN D-8514, Aug. 1977.

[16]Evans, R. J., "Aircraft Flight Data Compatibility Checking Using Maximum Likelihood and Extended Kalman Filter Estimation," *Proceedings of the 7th IFAC Symposium on Identification and System Parameter Estimation*, Pergamon Press, Oxford, England, UK, 1985, pp. 487–492.

[17]Parameswaran, V., Jategaonkar, R. V., and Press, M., "Calibration of Five-Hole Probe for Flow Angles from Dynamic and Tower Fly-by Maneuvers," AIAA Paper 2002-4627, Aug. 2002.

[18]De Leo, R. V., and Hagen, F. W., "Aerodynamic Performance of Rosemount Model 858AJ Air Data Sensor," Rosemount, Rept. 8767, Minneapolis, Minnesota, July 1976.

[19]Mulder, J. A., Baarspul, M., Breeman, J. H., Nieuwpoort, A. M., Verbraak, J. P. T., and Steeman, P. S. J. M., "Determination of the Mathematical Model for the New Dutch Government Civil Aviation Flying School Flight Simulator," *Proceeding of the 18th Annual Symposium of the Society of Flight Test Engineers*, Society of Flight Test Engineers, Amsterdam, The Netherlands, 1987.

[20]Baillie, S. W., Hui, K., and DeLeeuw, J., "The Flight Test and Data Analysis Program for the Development of a Boeing/deHavilland Dash 8 Simulator Model," AGARD CP-519, Paper 30, Oct. 1992.

[21]Neville, K. W., and Stephens, A. T., "Flight Update of Aerodynamic Math Model," AIAA Paper 93-3596, Aug. 1993.

[22]Jategaonkar, R. V., Moennich, W., Fischenberg, D., and Krag, B., "Identification of C-160 Simulator Data Base from Flight Data," *Proceedings of the 10th FAC Symposium on System Identification*, IFAC, Copenhagen, July 1994, pp. 1031–1038.

[23]Trankle, T. L., and Bachner, S. D., "Identification of a Nonlinear Aerodynamic Model of the F-14 Aircraft," *Journal of Guidance, Control, and Dynamics*, Vol. 18, No. 6, 1995, pp. 1292–1297.

[24]Jategaonkar, R. V., and Moennich, W., "Identification of DO-328 Aerodynamic Database for a Level D Flight Simulator," AIAA Paper 97-3729, Aug. 1997.

[25]Jategaonkar, R. V., Moennich, W., Fischenberg, D., and Krag, B., "Identification of Speed Brake, Air-Drop and Landing Gear Effects from Flight Data," *Journal of Aircraft*, Vol. 34, No. 2, 1997, pp. 174–180.

[26]Weiss, S., Gockel, W., Moennich, W., and Rohlf, D., "Identification of Dornier-328 Reversible Flight Control Systems," AIAA Paper 98-4163, Aug. 1998.

[27]Jategaonkar, R. V., "Identification of Actuation System and Aerodynamic Effects of Direct-Lift-Control Flaps," *Journal of Aircraft*, Vol. 30, No. 5, 1993, pp. 636–643.

[28]Leishman, J. G., and Nguyen, K. Q., "State Space Representation of Unsteady Airfoil Behavior," *AIAA Journal*, Vol. 28, No. 5, 1990, pp. 836–844.

[29]Fischenberg, D., "Identification of an Unsteady Aerodynamic Stall Model from Flight Test Data," AIAA Paper 95-3438, Aug. 1995.

[30]Goman, M., and Khrabrov, A., "State-Space Representation of Aerodynamic Characteristics of an Aircraft at High Angles of Attack," *Journal of Aircraft*, Vol. 31, No. 5, 1994, pp. 1109–1115.

[31]Ray, P. A., "Federal Aviation Administration Flight Simulation Standards—A Regulatory Update," AIAA Paper 95-3389, Aug. 1995.

[32]Weiss, S., Friehmelt, H., Plaetschke, E., and Rohlf, D., "X-31A System Identification Using Single-Surface Excitation at High Angles of Attack," *Journal of Aircraft*, Vol. 33, No. 3, 1996, pp. 485–490.

[33]Jategaonkar, R. V., and Thielecke, F., "Evaluation of Parameter Estimation Methods for Unstable Aircraft," *Journal of Aircraft*, Vol. 31, No. 3, 1994, pp. 510–519.

[34]Schawe, D., Rohardt, C.-H., and Wichmann, G., "Aerodynamic Design Assessment of Strato 2C and Its Potential for Unmanned High Altitude Airborne Platforms," *Journal of Aerospace Science and Technology*, Vol. 6, No. 1, 2002, pp. 43–51.

[35]Fischenberg, D., "Identification of STRATO 2C Aerodynamic Data Base—Part 1: Low Speed, 0-30000 ft," DLR, IB 111-95/23, Braunschweig, Germany, July 1995.

[36]Pete, K. R., Smith, S. T., and Vicroy, D., "Model Validation of Wake-Vortex/Aircraft Encounters," AIAA Paper 2000-3979, Aug. 2000.

[37]Fischenberg, D., "S-WAKE: Results of Flight Test Data Analysis," DLR, IB 111-2002/11, Braunschweig, Germany, Sept. 2002.

[38]Burnham, D. C., and Hallock, J. N., *Chicago Monoacoustic Vortex Sensing System, Wake Vortex Decay*, Vol. 4, National Technical Information Service, Springfield, VA, 1982.

[39]Lamb, H., *Hydrodynamics*, Cambridge Univ. Press, Cambridge, England, U.K., 1932, pp. 590–592.

[40]Fischenberg, D., "Bestimmung der Wirbelschlep pencharakteristik aus Flugmessdaten," Deutscher Luft- und Raumfahrtkongress, Paper DGLR-2002-170, Sept. 2002 (in German).

[41]Fischenberg, D., and Rohlf, D., "Identifizierung der Einflüsse von Kompressibilität und Strukturelastizität auf die Aerodynamischen Derivative eines Widebody-Verkehrsflugzeugs," DLR-IB 111-98/03, Braunschweig, Germany, Jan. 1998 (in German).

[42]Hamel, P. G., and Jategaonkar, R. V., "The Role of System Identification for Flight Vehicle Applications—Revisited," RTO-MP-11, Paper 2, March 1999.

[43]Pitt, D. M., and Peters, D. A., "Theoretical Prediction of Dynamic Inflow Derivatives," Vertica, Pergamon, Oxford, England, UK, Vol. 5, No. 1, 1981, pp. 21–34.

[44]Hamers, M., and von Gruenhagen, W., "Nonlinear Helicopter Model Validation Applied to Real Time Simulations," *Proceedings of the 53rd Annual AHS Forum*, Vol. 2, American Helicopter Society, Alexandria, VA, 1997, pp. 958–972.

[45]Kraemer, P., Gimonet, B., and von Gruenhagen, W., "A Systematic Approach to Nonlinear Rotorcraft Model Identification," *Journal of Aerospace Science and Technology*, Vol. 6, No. 8, 2002, pp. 579–590.

[46]Theodore, C., and Celi, R., "Helicopter Flight Dynamic Simulation with Refined Aerodynamics and Flexible Blade Modeling," *Journal of Aircraft*, Vol. 39, No. 4, 2002, pp. 577–586.